How to cite: *Angew. Chem. Int. Ed.* **2020**, *59*, 9382–9387
International Edition: doi.org/10.1002/anie.202002309
German Edition: doi.org/10.1002/ange.202002309

VIP Batteries Very Important Paper

An Adjustable-Porosity Plastic Crystal Electrolyte Enables High-Performance All-Solid-State Lithium-Oxygen Batteries

*Jin Wang[+], Gang Huang[+], Kai Chen, and Xin-Bo Zhang**

Abstract: *The limited triple-phase boundaries (TPBs) in solid-state cathodes (SSCs) and high resistance imposed by solid electrolytes (SEs) make the achievement of high-performance all-solid-state lithium-oxygen (ASS Li-O_2) batteries a challenge. Herein, an adjustable-porosity plastic crystal electrolyte (PCE) has been fabricated by employing a thermally induced phase separation (TIPS) technique to overcome the above tricky issues. The SSC produced through the in-situ introduction of the porous PCE on the surface of the active material, facilitates the simultaneous transfer of Li^+/e^-, as well as ensures fast flow of O_2, forming continuous and abundant TPBs. The high Li^+ conductivity, softness, and adhesion of the dense PCE significantly reduce the battery resistance to 115 Ω. As a result, the ASS Li-O_2 battery based on this adjustable-porosity PCE exhibits superior performances with high specific capacity (5963 mAh g^{-1}), good rate capability, and stable cycling life up to 130 cycles at 32 °C. This novel design and exciting results could open a new avenue for ASS Li-O_2 batteries.*

Lithium-oxygen (Li-O_2) batteries have been attracting worldwide attention as a possible green alternative to current commercial lithium-ion (Li-ion) batteries due to their ultra-high theoretical energy density (3500 Wh kg^{-1}).[1] Instead of the major problems, like evaporation, leakage, and flammability, encountered in conventional Li-O_2 batteries with organic electrolytes (OE), all-solid-state (ASS) Li-O_2 batteries with solid electrolytes (SEs) provide potential solutions to conquer these.[2] Despite their good prospects, ASS Li-O_2 batteries are still in their infancy and lots of scientific and technological problems, like limited triple-phase boundaries (TPBs) in the solid-state cathode (SSC), large resistance, and poor stability of SEs, need to be solved.[3]

A typical ASS Li-O_2 battery consists of a Li anode, a SE and a SSC.[4] Being different from conventional cathodes, SSCs in ASS Li-O_2 batteries require a large number of TPBs (Li^+, e^-, O_2), serving as active sites, to facilitate the electrochemical reaction proceeding, thus it is necessary to introduce the SE into the SSC.[5] Moreover, the diffusion of O_2 demands the SSC to be porous, while the transfer of Li^+ requires the SE inside the SSC to be in a continuous state. These two conflicting requirements make the design of satisfactory SSCs really a challenging task. At present, the main method for constructing SSCs is to mix the SE and electronic conductor by methods such as ball milling or sintering.[6] The TPBs created by this method are very limited because the transfer of Li^+ and e^- is discontinuous, and the diffusion of O_2 is hindered, which causes ASS Li-O_2 batteries with low capacity (<4500 mAh g^{-1}) and poor cycle life (≤ 10 cycles). Therefore, the development of a facile and effective strategy to construct a SSC with abundant TPBs to overcome all the above issues is highly desired.

The commonly used SEs can be classified into two major types, ceramic electrolytes (CEs) and polymer electrolytes (PEs).[7] CEs, represented by Na^+ superionic conductor and garnet, have a high Young's modulus and lithium-ion transfer number.[8] Although the room temperature ionic conductivity of some CEs can reach 10^{-3} S cm^{-1}, their large thickness and rigidness make the electrolyte resistance and interface resistance against electrodes ($>10^3$ Ω) too high to enable a high-performance solid battery.[9] Poly(ethylene oxide) (PEO) is the most widely studied PE due to its flexibility and easy preparation. Unfortunately, its room temperature ionic conductivity is poor (10^{-7} S cm^{-1}), as a result, the PEO-based batteries cannot operate at room temperature owing to the large electrolyte resistance.[10] Current works address this problem by increasing the battery operating temperature or adding an OE wetting layer.[11] Although these methods are effective to some extent, new security risks, high temperature and OE, are introduced. To the best of our knowledge, no SE has yet been able to enable a high-performance ASS Li-O_2 battery at room temperature.

Considering that the structural disorder of plastic crystals can lead to good plasticity and enhanced ion diffusivity,[12] the plastic crystal electrolytes (PCEs), a mixture of lithium salts and plastic crystals, have a strong ability to transfer Li^+. Therefore, succinonitrile (SN)-based PCE, a representative PCE, with high room temperature ionic conductivity up to 10^{-3} S cm^{-1} has been successfully applied in ASS Li-ion batteries, while its use in ASS Li-O_2 batteries is rare.[13] Conventionally, SN-based PCE has long been obtained by

[*] J. Wang,[+] K. Chen, Prof. X.-B. Zhang
State Key Laboratory of Rare Earth Resource Utilization, Changchun Institute of Applied Chemistry, Chinese Academy of Sciences
Changchun, 130022 (P. R. China)
E-mail: xbzhang@ciac.ac.cn
J. Wang[+]
Key Laboratory of Automobile Materials, Ministry of Education, Department of Materials Science and Engineering, Jilin University
Changchun, 130022 (P. R. China)
Dr. G. Huang[+]
Materials Science and Engineering, Physical Science and Engineering Division
King Abdullah University of Science and Technology (KAUST)
Thuwal, 23955-6900 (Saudi Arabia)
[+] These authors contributed equally to this work.
Supporting information and the ORCID identification number(s) for the author(s) of this article can be found under: https://doi.org/10.1002/anie.202002309.

solvent evaporation or UV-curing method, wherein SN is dissolved by solvent or heating and then solidified.[14] However, since only a uniform solution phase is formed in these methods, the morphology of the obtained SN-based electrolyte is always dense, which cannot fulfill the requirements of constructing abundant TPBs in ASS Li-O_2 batteries. Thus, it is challenging yet urgent to rationally introduce the SN-based PCE into the ASS Li-O_2 batteries according to local conditions.

In this work, inspired by the fact that thermally induced phase separation (TIPS) is a simple and controllable phase separation process,[15] for the first time, we propose TIPS as a novel porous membrane formation technique for the construction of adjustable-porosity SN-based PCEs. On the one hand, the in-situ introduction of porous SN-based electrolyte on the surface of the carbon cathode enables simultaneous Li^+/e^- transfer and fast diffusion of O_2, constructing a SSC with abundant and continuous TPBs. On the other hand, the resistance of the ASS Li-O_2 battery has been significantly reduced by adopting dense SN-based PCE due to its fantastic Li^+ conductivity, softness and adhesion. Thanks to these advantages, the ASS Li-O_2 batteries based on adjustable-porosity SN-based PCE show high discharge capacity, superior rate performance, and long cycle life.

Figure 1a displays the synthesis process of the SN-based PCE by TIPS with a composition of SN, lithium bis(trifluoromethanesulphonyl)imide (LiTFSI), poly(vinylidene fluoride-hexafluoropropylene) (PVDF-HFP), and 2,6-di-tert-butyl-4-methylphenol (BHT) (denoted as SLPB). The solvent used is DMSO. The additions of PVDF-HFP and BHT are to improve the poor mechanical strength and the antioxidant ability of SN, respectively.[16] The detailed synthesis process is as follows: First, all the raw materials are dissolved in DMSO at 60 °C. Subsequently, the obtained solution is poured on a glass plate and quenched at 30 °C. The temperature discrepancy during this process will cause solid–liquid phase separation. Finally, the SLPB is obtained after evaporating the DMSO solvent. In the field of TIPS, the solution concentration is a critical parameter that would greatly influence the process of phase separation, then further change the morphology of the membrane. Theoretically, the number of pores on the obtained membrane is inversely proportional to the solution concentration.[17] With this in mind, different amounts of DMSO (2/3/4 mL) were used to adjust the porosity of SLPB (denoted as SLPB2/3/4). As can be seen from the SEM images in Figure 1b–d, the amount of DMSO significantly influences the morphology and porosity of SLPB. The SLPB becomes more and more porous with the increase of DMSO amount and the porosity of SLPB2/3/4 is 0.61 %, 20.76 % and 46.25 %, respectively, which is consistent with the theory prediction.

As indicated in Figure 2a, although the porosities of SLPB2-4 are different, their phases are almost identical, indicating that the amount of DMSO does not change the composition of SLPB and only adjusts the porosity. Since the Li^+ conduction in electrolyte is achieved by the continuous transfer of Li^+, the porosity of SLPB will affect its ionic conductivity. As shown in Figure 2b and Figure S1 in the Supporting Information, even with the significant increase of porosity from 0.61 % to 46.25 %, the ionic conductivity of SLPB experiences a slight decrease from 3.87×10^{-4} S cm^{-1} to 2.43×10^{-4} S cm^{-1}, revealing that the existence of a large amount of pores in SLPB will not cut off the continuous transfer properties of Li^+, demonstrating the advantage of the designed SLPB. Due to the highest ionic conductivity, SLPB2 was selected for detailed characterization. Since the mechanical characters of SE are critical to form close interface contact against electrodes, the Young's modulus and adhesion property of SLPB2 have been tested by AFM.[18] PEO

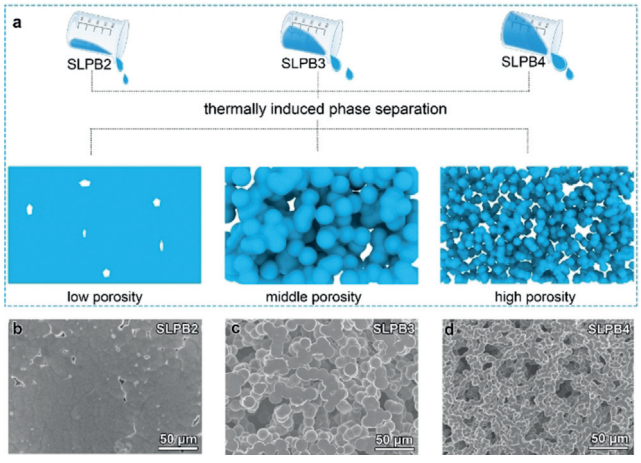

Figure 1. a) Schematic illustration of the preparation of SLPB. SEM images of b) SLPB2, c) SLPB3, and d) SLPB4.

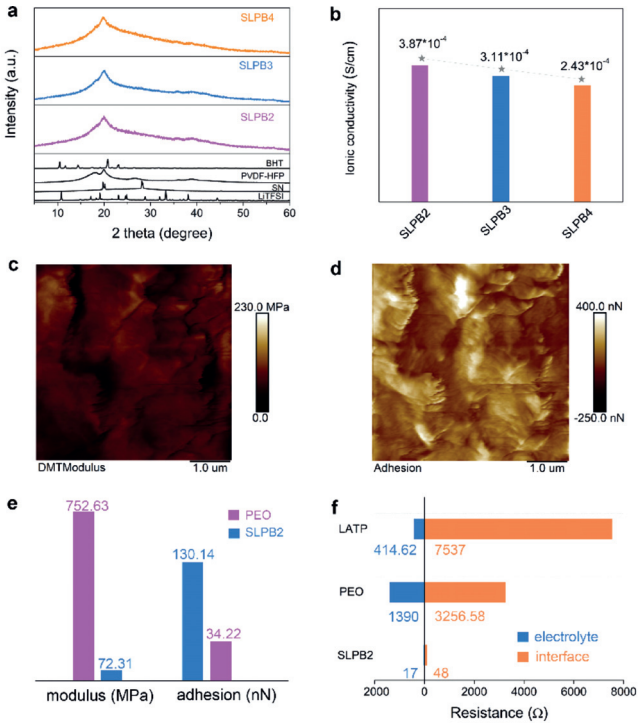

Figure 2. a) XRD patterns and b) ionic conductivity of SLPB. c) Young's modulus and d) adhesion mappings of SLPB2. e) Specific values of the Young's modulus and the adhesion of PEO and SLPB2. f) Resistance values of symmetric LiF-Li/LiF-Li batteries with LATP, PEO, and SLPB2.

(Figure S2), as a representative flexible PE, has also been tested for comparison. It is clear that the Young's modulus of SLPB2 is much lower than that of PEO (Figure 2c and Figure S3a), which means the SLPB2 is substantially softer than PEO. Even with high softness, the SLPB2 can still form a free-standing membrane with excellent bendability (Figure S4). As indicated in Figure 2d and Figure S3b, the SLPB2 exhibits a stronger adhesion than that of PEO. To more clearly observe the difference between SLPB2 and PEO, the specific values of modulus and adhesion are given in Figure 2e. The Young's modulus of SLPB2 is 9-fold lower than that of PEO (72.31 vs. 752.63 MPa), while, the adhesion of SLPB2 is about 4-fold higher than that of PEO (130.14 nN vs. 34.22 nN). The high softness and firm adhesion of SLPB2 are beneficial to form tight interface contact and decrease interface resistance.

In order to confirm the ability of the SLPB2 in decreasing the interface resistance, electrochemical impedance spectra (EIS) tests of symmetric LiF-protected Li/LiF-protected Li (LiF-Li/LiF-Li) batteries with $Li_{1.3}Al_{0.3}Ti_{1.7}(PO_4)_3$ (LATP), PEO and SLPB2 electrolytes were performed. LATP (Figure S5), as a representative CE, was tested as another control sample for its wide applications in solid-state batteries. Instead of Li, LiF-Li was used to construct the symmetric cells due to its excellent stability against electrolyte (Figures S6 and S7).[19] In contrast to batteries with LATP and PEO, the SLPB2-based battery shows the smallest resistance (Figure S8 and Table S1). Although the ionic conductivity of SLPB2 is just slightly higher than that of LATP (Figure S9 and Table S2), the electrolyte resistance and interface resistance of SLPB2 are both much lower than those of LATP (Figure 2f) because SLPB2 is thin and soft while LATP is thick and rigid. For PEO, the poor ionic conductivity makes it exhibit the highest electrolyte resistance. While the flexibility of PEO enables a smaller interface resistance than that of LATP, it is still more than 100-fold higher than that of SLPB2. The smallest electrolyte and interface resistances of the SLPB2-based battery can be attributed to the opportune thickness, conductive ionic passways, softness, and adhesion of SLPB2.

Inspired by the above advantages, it is very promising to introduce SLPB into ASS Li-O_2 batteries to solve the problems of conventional ASS Li-O_2 batteries. As depicted in Figure 3a, taking conventional ASS Li-O_2 batteries with CE as an example, the interface contacts at both the anode and the SSC sides are poor because of the relatively stiff CE, resulting in a large interface resistance.[6b,c] Furthermore, the resistance of the CE itself cannot be ignored.[6a] All this makes the CE based ASS Li-O_2 batteries exhibit a large resistance. For the commonly used SSC in conventional ASS Li-O_2 batteries, the contact between Li^+ conductor and e^- conductor is almost point-to-point, and O_2 cannot diffuse sufficiently due to the lack of reasonably designed gas diffusion channels, so the TPBs in the SSCs of conventional ASS Li-O_2 batteries are very limited. In contrast, our design for an ASS Li-O_2 battery based on adjustable-porosity SLPB can simultaneously resolve the above issues. The dense SLPB electrolyte layer can deliver high Li^+ conductivity and enable close contact with electrodes (Figure 3b), achieving low cell

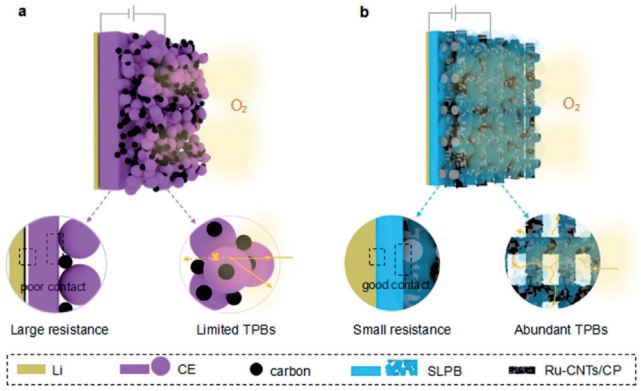

Figure 3. Schematic illustration of a) the conventional ASS Li-O_2 battery with CE and b) the ASS Li-O_2 battery with adjustable-porosity SLPB.

resistance. The SSCs prepared by in-situ introducing SLPB2/3/4 into Ru-carbon nanotubes (Ru-CNTs) (Figure S10) cathodes (denoted as SLPBC2/3/4) realize simultaneous transfer of Li^+/e^- and leave abundant pores to allow sufficient and quick flow of O_2 to form abundant TPBs. The simultaneous solution of the problems of high resistance and limited TPBs in conventional ASS Li-O_2 batteries by this ingenious design is promising to significantly improve the performance of ASS Li-O_2 batteries.

The above hypothesis can be checked by constructing ASS Li-O_2 batteries to test battery capabilities. To find the best SLPBC, discharge test was performed on SLPBC2/3/4 prepared by dripping different amounts of SLPB2/3/4 on Ru-CNTs cathodes. As shown in Figures S11–S13, for all the three SLPBC2-4, the addition of 80 μL of SLPB makes the ASS Li-O_2 batteries exhibit the largest discharge capacities. Therefore, in the following tests, 80 μL of SLPB was used in the preparation process of SLPBC. With these optimized SLPBC, the SLPBC3- and SLPBC4-based ASS Li-O_2 batteries deliver higher discharge capacities than that of SLPBC2 (5963 and 4924 vs. 2859 mAh g^{-1}, respectively), indicating that the structure of cathode has a significant influence on the discharge capacity. SEM was then used to observe the morphology of SLPBC. As displayed in Figure 4a–c, different from the dense structure of SLPBC2, both SLPBC3 and SLPBC4 exhibit porous configurations. The dense SLPBC2 with finite pores could impede O_2 transfer and only create limited TPBs, thus causing low discharge capacity. In sharp contrast, the numerous pores in SLPBC3 facilitate O_2 transfer, which is beneficial for producing abundant TPBs, to achieve high discharge capacity. Similarly, abundant TPBs can be created by the porous SLPBC4, but its relatively low ionic conductivity results in lower discharge capacity than that of SPLBC3, revealing that the porous architecture and the high ionic conductivity of SLPBC are both dispensable for delivering a large discharge capacity.

Apart from capacity, the rate capability of ASS Li-O_2 batteries is also closely related with the properties of SLPBC. Figure 4d displays the full discharge curves of ASS Li-O_2 batteries with SLPBC3 at various current densities. When the current density is increased from 200 mA g^{-1} to 500 mA g^{-1},

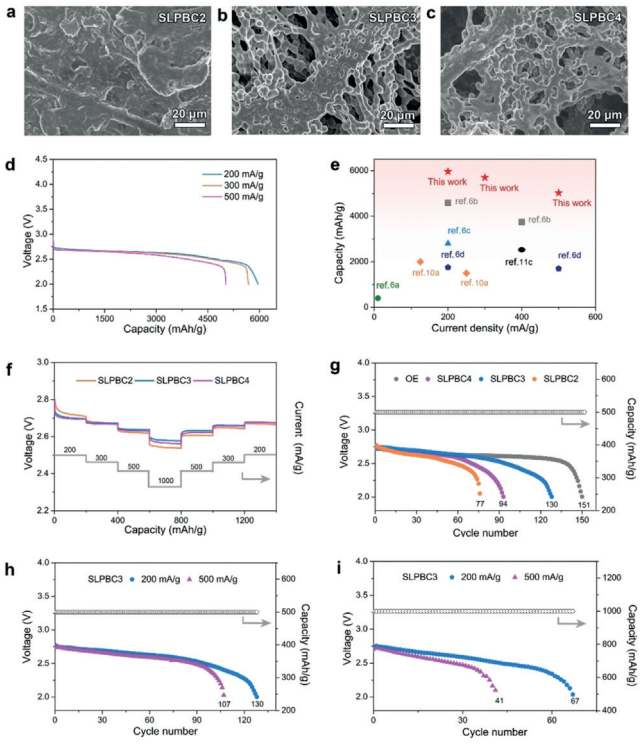

Figure 4. SEM images of a) SLPBC2, b) SLPBC3, and c) SLPBC4. d) Full discharge curves of ASS Li-O_2 batteries with SLPBC3 at various current densities. e) Comparison of the discharge capacities of SLPBC3 based batteries with some previously reported ASS Li-O_2 batteries. f) Rate performance of ASS Li-O_2 batteries with different SLPBC. g) Cycle life of ASS Li-O_2 batteries with different SLPBC at a current density of 200 mA g^{-1} with a fixed capacity of 500 mAh g^{-1}. Cycle life of ASS Li-O_2 batteries with SLPBC3 at different current densities with fixed capacities of h) 500 mAh g^{-1} and i) 1000 mAh g^{-1}.

the discharge voltage platform keeps stable, and the discharge capacity only slightly decreases. It is worth noting that the ASS Li-O_2 battery with SLPBC3 has the highest discharge capacity compared with other reported works at any current densities (Figure 4e). Even using pure CNTs as the cathode, the ASS Li-O_2 battery still exhibits a high discharge capacity above 5000 mAh g^{-1} (Figure S14), around 1000 mAh g^{-1} lower than that of the ASS Li-O_2 battery with Ru-CNTs cathode, indicating that the TPBs rather than the catalyst play a more important role on the discharge capacity. Furthermore, the SLPBC3 based ASS Li-O_2 battery exhibits a resistance of only 115 Ω at 32 °C, the smallest value reported to date in this field, much smaller than the resistances of above 10^3 Ω at room temperature and circa 360 Ω at 80 °C for reported ASS Li-O_2 batteries (Figure S15 and Table S3).[10a] Furthermore, the resistance of ASS Li-O_2 battery with SLPBC3 is comparable to that of the Li-O_2 battery with OE. To observe the influence of TPBs on rate performance, the discharge voltage platforms of ASS Li-O_2 batteries with SLPBC2/3/4 at different current densities were checked. As shown in Figure 4f, the discharge voltage plateau of SLPBC3 is always higher than that of SLPBC4 and exhibits the smallest polarization alteration even with the rapid change of current density for every 200 mAh g^{-1}. The high ionic conductivity of SLPBC2 makes it show the highest voltage platform at the beginning of the discharge. However, as the discharge progresses, the limited TPBs induced by its dense structure quickly deteriorate the rate performance, even poorer than that of SLPBC4. It should be noted that the achieved superior capacity and rate performance of SLPBC3 based ASS Li-O_2 battery can be attributed to the following advantages: 1) The high ionic conductive, soft, and sticky SLPB2 endows an ultra-low resistance for ASS Li-O_2 battery, ensuring low polarization during discharge/charge and 2) the continuous and abundant TPBs in SLPBC3 provide ample active sites for the electrochemical reaction, which are helpful to increase discharge capacity and achieve good rate performance.

Another significant feature of the ASS Li-O_2 battery with SLPBC3 is the cycling stability. Figure 4g presents the terminal voltage versus cycle number profiles of ASS Li-O_2 batteries with SLPBC2/3/4 cycled at 200 mA g^{-1} with a fixed capacity of 500 mAh g^{-1}. The SLPBC3-based ASS Li-O_2 battery can realize 130 stable cycles before reaching the cut off voltage of 2 V, which is the longest cycle life of ASS Li-O_2 battery ever reported (Table S4). In contrast, the discharge terminal voltages of the SLPBC2- and SLPBC4-based batteries degrade to 2 V only after 77 and 94 cycles, respectively. The SLPBC3-based ASS Li-O_2 battery also shows the lowest discharge–charge overpotential than those of SLPBC2- and SLPBC4-based batteries (Figure S16). These results confirm that the presence of continuous and abundant TPBs is vital for the long-term stability of ASS Li-O_2 batteries. Notably, the cycle life of ASS Li-O_2 battery with SLPBC3 can even be comparable to that of Li-O_2 battery with OE (130 vs. 151 cycles). Moreover, with the increase of current density to 500 mA g^{-1}, the ASS Li-O_2 battery with SLPBC3 can still run stable for up to 107 cycles (Figure 4h), further certifying its superior rate capability. Even increased the cycling capacity to 1000 mAh g^{-1} (Figure 4i), the ASS Li-O_2 battery with SLPBC3 shows better cycle life compared with other reported works at both 200 and 500 mA g^{-1}.

In order to understand the formation–decomposition processes of the discharge products in ASS Li-O_2 batteries, the evolution of cathode was observed by SEM. As presented in Figure 5a, after the first discharge, spherical or toroid-like discharge products with sizes of hundreds of nanometers distribute along the Ru-CNTs. After subsequent recharge, the discharge products disappear (Figure 5b), and the surface of the Ru-CNTs becomes clear to its pristine state (Figure S17), indicating the complete decomposition of the discharge products. The phase of the discharge product was characterized by XRD. As shown in Figure 5c, except the peaks corresponding to Ru-CNTs, all the other peaks of the discharged cathode can be ascribed to Li_2O_2, and it disappears completely after recharging. The above results indicate that the ASS Li-O_2 batteries with SLPC3 follow the typical Li_2O_2 formation–decomposition pathway like OE-based Li-O_2 batteries and permit the electrochemical reactions to proceed in a highly reversible manner.[13e]

Despite the superior cycling performance of the ASS Li-O_2 battery with SLPBC3, it still fails after 130 cycles. To unveil the hidden reasons, XRD, Raman spectroscopy, and SEM

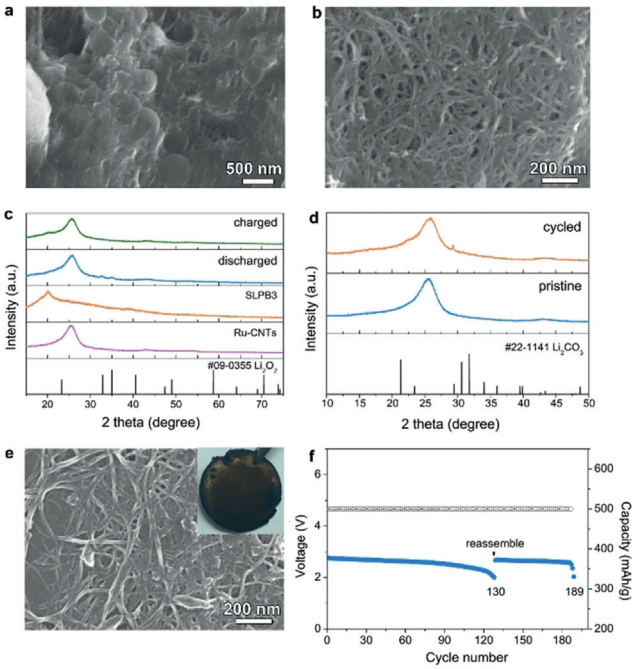

Figure 5. a) SEM image of the SLPBC3 after discharging a capacity of 1000 mAh g^{-1}. b) SEM image of the recharged SLPBC3. c) XRD patterns of the pristine, discharged, and recharged SLPBC3. d) XRD pattern and e) SEM image of the SLPBC3 disassembled from ASS Li-O_2 batteries after 130 cycles. Inset: The cycled SLPBC3 before washing by DMSO. f) Cycle life of the reassembled ASS Li-O_2 battery at a current density of 200 mA g^{-1} with a fixed capacity of 500 mAh g^{-1}.

have been employed to analyze the cycled SLPBC3 because side products are easily accumulated there.[20] According to XRD patterns, the side product on the cycled SLPBC3 can be identified as Li_2CO_3 (Figure 5d), which can be further confirmed by the appearance of Li_2CO_3 peak at 1090 cm^{-1} in the Raman spectra of the cycled SLPBC3 (Figure S18).[21] In addition, the SEM image clearly shows that the clean network of the pristine SLPBC3 is absolutely covered by Li_2CO_3 after the battery failed (Figure 5e). These results suggest that the accumulated Li_2CO_3 on the SLPBC3 is responsible for the death of ASS Li-O_2 battery. Apart from the formation of Li_2CO_3 byproduct, the instability of SLPBC3 is also observed. The fresh SLPBC3 is white (Figure S19), however, it turns brown after cycling (inset of Figure 5e). In consideration of the strong oxidation environment in Li-O_2 batteries, the stability of SLPB towards the highly reactive reduced oxygen species (O_2^{2-} and O_2^-) has been checked. As indicated in Figure S20a, with the addition of pale-yellow KO_2, the transparent and colorless SN changes to a black solution, while the addition of white Li_2O_2 to SN just get a white solution without any O_2^{2-}-induced color change. It can be concluded that SN is stable with O_2^{2-}, but unstable with O_2^-. In the presence of BHT, the solution of SN is pale-yellow after adding KO_2, indicating that BHT can improve the stability of SLPB towards O_2^- (Figure S20b). Regrettably, the color of the solution turns from pale-yellow to brown when extending the test time (Figure S20c). Therefore, BHT can only alleviate the decomposition of SN to a certain extent. Based on these results, the accumulation of Li_2CO_3 together with the O_2^--induced decomposition of SLPB causes battery failure. To further verify this, the ASS Li-O_2 battery after running for 130 cycles is reassembled with a fresh SLPBC3 into a new battery (Figure 5f). The reassembled battery runs for another 59 cycles with almost the same terminal discharge voltage as the original battery, which indicates that solving the stability issue of cathodes and SEs is necessary for further improving the performance of ASS Li-O_2 batteries.

In summary, an adjustable-porosity PCE with features of high ionic conductivity, excellent softness and adhesion has been prepared for the first time with the help of a simple and easily controllable TIPS method. When using dense PCE as SE and in-situ introducing porous PCE on the cathode surface, the serious issues of large resistance and limited TPBs for ASS Li-O_2 batteries are successfully solved. As a result, the ASS Li-O_2 battery exhibits promising performance, including ultra-low resistance, large capacity, good rate capability, and long cycle life. This appealing adjustable-porosity electrolyte preparation technology as well as the excellent electrochemical results lead to a new avenue for the development of ASS Li-O_2 batteries.

Acknowledgements

This work was financially supported by the National Key R&D Program of China (2017YFA0206700), the National Natural Science Foundation of China (21725103 and 21905269), the Strategic Priority Research Program of the Chinese Academy of Sciences (XDA21010210), Jilin Province Science and Technology Development Plan Funding Project (20180101203JC), Jilin Province Capital Construction Funds Project (2020C026-1), Changchun Science and Technology Development Plan Funding Project (19SS010, 18DY012)and the K. C. Wong Education Foundation (GJTD-2018-09).

Conflict of interest

The authors declare no conflict of interest.

Keywords: all-solid-state · lithium-oxygen batteries · plastic crystal electrolytes · solid electrolytes · succinonitrile

[1] a) M. Asadi, B. Sayahpour, P. Abbasi, A. T. Ngo, K. Karis, J. R. Jokisaari, C. Liu, B. Narayanan, M. Gerard, P. Yasaei, X. Hu, A. Mukherjee, K. C. Lau, R. S. Assary, F. Khalili-Araghi, R. F. Klie, L. A. Curtiss, A. Salehi-Khojin, *Nature* **2018**, *555*, 502 – 506; b) C. Xia, C. Y. Kwok, L. F. Nazar, *Science* **2018**, *361*, 777 – 781.

[2] a) Y. Qiao, K. Z. Jiang, H. Deng, H. S. Zhou, *Nat. Catal.* **2019**, *2*, 1035 – 1044; b) J. Q. Zhang, B. Sun, Y. F. Zhao, A. Tkacheva, Z. J. Liu, K. Yan, X. Guo, A. M. McDonagh, D. Shanmukaraj, C. Y. Wang, T. Rojo, M. Armand, Z. Q. Peng, G. X. Wang, *Nat. Commun.* **2019**, *10*, 602.

[3] a) J. N. Lai, Y. Xing, N. Chen, L. Li, F. Wu, R. J. Chen, *Angew. Chem. Int. Ed.* **2020**, *59*, 2974 – 2997; *Angew. Chem.* **2020**, *132*, 2994 – 3019; b) C. S. Yang, K. N. Gao, X. P. Zhang, Z. Sun, T. Zhang, *Rare Met.* **2018**, *37*, 459 – 472; c) L. L. Luo, B. Liu, S. D.

Song, W. Xu, J. G. Zhang, C. M. Wang, *Nat. Nanotechnol.* **2017**, *12*, 535 – 539.
[4] a) Y. J. Liu, P. He, H. S. Zhou, *Adv. Energy Mater.* **2018**, *8*, 1701602; b) B. Kumar, J. Kumar, R. Leese, J. P. Fellner, S. J. Rodrigues, K. M. Abraham, *J. Electrochem. Soc.* **2010**, *157*, A50 – A54.
[5] a) S. Wang, J. Wang, J. J. Liu, H. C. Song, Y. J. Liu, P. F. Wang, P. He, J. Xu, H. S. Zhou, *J. Mater. Chem. A* **2018**, *6*, 21248 – 21254; b) J. Y. Sun, N. Zhao, Y. Q. Li, X. X. Guo, X. F. Feng, X. S. Liu, Z. Liu, G. L. Cui, H. Zheng, L. Gu, H. Li, *Sci. Rep.* **2017**, *7*, 41217.
[6] a) H. Kitaura, H. S. Zhou, *Adv. Energy Mater.* **2012**, *2*, 889 – 894; b) Y. J. Liu, B. J. Li, Z. Cheng, C. Li, X. Y. Zhang, S. H. Guo, P. He, H. S. Zhou, *J. Power Sources* **2018**, *395*, 439 – 443; c) Y. J. Liu, B. J. Li, H. Kitaura, X. P. Zhang, M. Han, P. He, H. S. Zhou, *ACS Appl. Mater. Interfaces* **2015**, *7*, 17307 – 17310; d) H. Kitaura, H. S. Zhou, *Energy Environ. Sci.* **2012**, *5*, 9077 – 9084.
[7] L. Fan, S. Y. Wei, S. Y. Li, Q. Li, Y. Y. Lu, *Adv. Energy Mater.* **2018**, *8*, 1702657.
[8] a) T. Famprikis, P. Canepa, J. A. Dawson, M. S. Islam, C. Masquelier, *Nat. Mater.* **2019**, *18*, 1278 – 1291; b) A. J. Samson, K. Hofstetter, S. Bag, V. Thangadurai, *Energy Environ. Sci.* **2019**, *12*, 2957 – 2975; c) B. B. Wu, S. Y. Wang, J. Lochala, D. Desrochers, B. Liu, W. Q. Zhang, J. H. Yang, J. Xiao, *Energy Environ. Sci.* **2018**, *11*, 1803 – 1810; d) B. C. Zhang, L. Chen, J. K. Hu, Y. C. Liu, Y. F. Liu, Q. Feng, G. N. Zhu, L. Z. Fan, *J. Power Sources* **2019**, *442*, 227230; e) L. Chen, Y. T. Li, S. P. Li, L. Z. Fan, C. W. Nan, J. B. Goodenough, *Nano Energy* **2018**, *46*, 176 – 184.
[9] a) X. G. Han, Y. H. Gong, K. Fu, X. F. He, G. T. Hitz, J. Q. Dai, A. Pearse, B. Y. Liu, H. Wang, G. Rubloff, Y. F. Mo, V. Thangadurai, E. D. Wachsman, L. B. Hu, *Nat. Mater.* **2016**, *16*, 572 – 579; b) X. B. Cheng, C. Z. Zhao, Y. X. Yao, H. Liu, Q. Zhang, *Chem* **2019**, *5*, 74 – 96; c) F. D. Han, A. S. Westover, J. Yue, X. L. Fan, F. Wang, M. F. Chi, D. N. Leonard, N. J. Dudney, H. Wang, C. S. Wang, *Nat. Energy* **2019**, *4*, 187 – 196; d) J. Y. Wen, Y. Huang, J. Duan, Y. M. Wu, W. Luo, L. H. Zhou, C. C. Hu, L. Q. Huang, X. Y. Zheng, W. J. Yang, Z. Y. Wen, Y. H. Huang, *ACS Nano* **2019**, *13*, 14549 – 14556.
[10] a) M. Balaish, E. Peled, D. Golodnitsky, E. Y. Eli, *Angew. Chem. Int. Ed.* **2015**, *54*, 436 – 440; *Angew. Chem.* **2015**, *127*, 446 – 450; b) J. Y. Wan, J. Xie, X. Kong, Z. Liu, K. Liu, F. F. Shi, A. Pei, H. Chen, W. Chen, J. Chen, X. K. Zhang, L. Q. Zong, J. Y. Wang, L. Q. Chen, J. Qin, Y. Cui, *Nat. Nanotechnol.* **2019**, *14*, 705 – 711.
[11] a) K. F. Zhang, S. J. Mu, W. Liu, D. Zhu, Z. D. Ding, Y. G. Chen, *Ionics* **2018**, *25*, 25 – 33; b) H. T. T. Le, D. T. Ngo, P. N. Didwal, J. G. Fisher, C. N. Park, I. D. Kim, C. J. Park, *J. Mater. Chem. A* **2019**, *7*, 3150 – 3160; c) W. Yu, C. J. Xue, B. K. Hu, B. Q. Xu, L. L. Li, C. W. Nan, *Energy Storage Mater.* **2019**, https://doi.org/10.1016/j.ensm.2020.02.001.
[12] P. J. Alarco, Y. Abu-Lebdeh, A. Abouimrane, M. Armand, *Nat. Mater.* **2004**, *3*, 476 – 481.
[13] a) Y. Lu, Y. C. Cai, Q. Zhang, L. J. Liu, Z. Q. Niu, J. Chen, *Chem. Sci.* **2019**, *10*, 4306 – 4312; b) Z. H. Lu, J. Yu, J. X. Wu, M. B. Effat, S. C. T. Kwok, Y. Q. Lyu, M. M. F. Yuen, F. Ciucci, *Energy Storage Mater.* **2019**, *18*, 311 – 319; c) H. C. Gao, L. G. Xue, S. Xin, K. Park, J. B. Goodenough, *Angew. Chem. Int. Ed.* **2017**, *56*, 5541 – 5545; *Angew. Chem.* **2017**, *129*, 5633 – 5637; d) U. H. Choi, B. M. Jung, *Macromol. Res.* **2018**, *26*, 459 – 465; e) Y. Liu, J. Yi, Y. Qiao, D. Wang, P. He, Q. Li, S. C. Wu, H. S. Zhou, *Energy Storage Mater.* **2018**, *11*, 170 – 175; f) T. L. Jiang, P. G. He, G. X. Wang, Y. Shen, C. W. Nan, L. Z. Fan, *Adv. Energy Mater.* **2020**, https://doi.org/10.1002/aenm.201903376; g) L. Z. Fan, Y. S. Hu, A. J. Bhattacharyya, J. Maier, *Adv. Funct. Mater.* **2007**, *17*, 2800 – 2807.
[14] a) K. H. Choi, S. J. Cho, S. H. Kim, Y. H. Kwon, J. Y. Kim, S. Y. Lee, *Adv. Funct. Mater.* **2014**, *24*, 44 – 52; b) D. Zhou, Y. B. He, R. L. Liu, M. Liu, H. D. Du, B. H. Li, Q. Cai, Q. H. Yang, F. Y. Kang, *Adv. Energy Mater.* **2015**, *5*, 1500353; c) H. J. Ha, E. H. Kil, Y. H. Kwon, J. Y. Kim, C. K. Lee, S. Y. Lee, *Energy Environ. Sci.* **2012**, *5*, 6491 – 6499; d) X. L. Wu, S. Xin, H. H. Seo, J. Kim, Y. G. Guo, J. S. Lee, *Solid State Ionics* **2011**, *186*, 1 – 6.
[15] a) K. S. McGuire, D. R. Lloyd, G. B. A. Lim, *J. Membr. Sci.* **1993**, *79*, 27 – 34; b) D. R. Lloyd, K. E. Kinzer, H. S. Tseng, *J. Membr. Sci.* **1990**, *52*, 239 – 261.
[16] a) W. Yu, W. Yang, R. L. Liu, L. Qin, Y. Lei, L. Liu, D. Y. Zhai, B. H. Li, F. Y. Kang, *Electrochem. Commun.* **2017**, *79*, 68 – 72; b) B. Nieva-Echevarría, M. J. Manzanos, E. Goicoechea, M. D. Guillen, *Compr. Rev. Food Sci. Food Saf.* **2015**, *14*, 67 – 80.
[17] A. California, V. F. Cardoso, C. M. Costa, V. Sencadas, G. Botelho, J. L. Gomez-Ribelles, S. Lanceros-Mendez, *Eur. Polym. J.* **2011**, *47*, 2442 – 2450.
[18] H. Duan, Y. X. Yin, Y. Shi, P. F. Wang, X. D. Zhang, C. P. Yang, J. L. Shi, R. Wen, Y. G. Guo, L. J. Wan, *J. Am. Chem. Soc.* **2018**, *140*, 82 – 85.
[19] a) Q. Q. Zhang, K. Liu, F. Ding, W. Li, X. J. Liu, J. L. Zhang, *ACS Appl. Mater. Interfaces* **2017**, *9*, 29820 – 29828; b) N. Xiao, G. Gourdin, Y. Y. Wu, *Angew. Chem. Int. Ed.* **2018**, *57*, 10864 – 10867; *Angew. Chem.* **2018**, *130*, 11030 – 11033; c) C. H. Wang, K. R. Adair, J. W. Liang, X. N. Li, Y. P. Sun, X. Li, J. W. Wang, Q. Sun, F. P. Zhao, X. T. Lin, R. Y. Li, H. Huang, L. Zhang, R. Yang, S. G. Lu, X. L. Sun, *Adv. Funct. Mater.* **2019**, *29*, 1900392.
[20] X. W. Gao, Y. H. Chen, L. R. Johnson, Z. P. Jovanov, P. G. Bruce, *Nat. Energy* **2017**, *2*, 17118.
[21] Z. H. Ni, H. M. Fan, Y. P. Feng, Z. X. Shen, B. J. Yang, Y. H. Wu, *J. Chem. Phys.* **2006**, *124*, 204703.

Manuscript received: February 13, 2020
Version of record online: April 14, 2020

